



**Warning and Mitigation technologies for Travelling Ionospheric Disturbances Effects**

**H2020-COMPET-2017**

# **Monitoring and analysis of the TIDs triggered by magnetic storms and their impact on EGNOS availability degradation**

**Dalia Buresova<sup>1</sup>, Anna Belehaki<sup>2</sup>, José Miguel Juan<sup>3</sup>, Jaume Sanz Subirana<sup>3</sup>, John Bosco Habarulema<sup>4</sup>, Zama Katamzi<sup>4</sup>, David Altadill<sup>5</sup>, Estefania Blanch<sup>5</sup>, Antoni Segarra<sup>5</sup>, Jurgen Watermann<sup>6</sup>, Ivan Galkin<sup>7</sup>, and TechTIDE team**

<sup>1</sup> Institute of Atmospheric Physics of the Czech Academy of Sciences, Prague, Czech Republic,

<sup>2</sup> National Observatory of Athens, IAASARS, Penteli, Greece,

<sup>3</sup> Universitat Politècnica de Catalunya, Barcelona, Spain,

<sup>4</sup> SANSA Space Science, Hermanus, South Africa

<sup>5</sup> University of Ramon Llull, Observatory Ebre, CSIC, Roquetes, Spain,

<sup>6</sup> JFWCONSULT, Tourrettes, France,

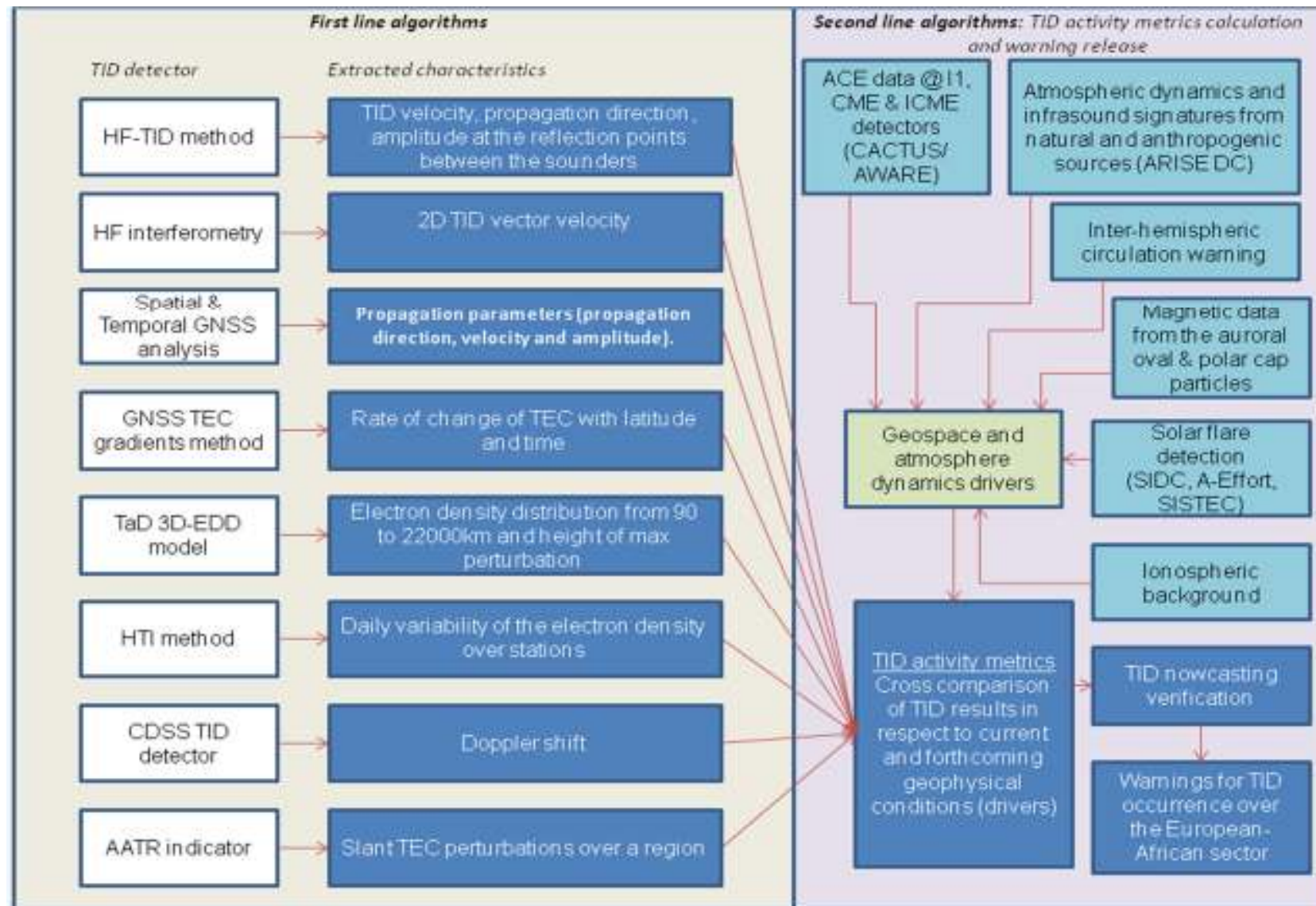
<sup>7</sup> University of Massachusetts Lowell, Space Science Laboratory, Lowell, MA USA



## Scope of the presentation:

- Brief introduction to the techniques applied to detection of LSTID
- Brief information on EGNOS
- Results of analysed space weather events
- Summary

## First and second line algorithms contribute to the TID activity metrics report and warnings



TID detection method	Brief description of the method
<b>HF-TID</b>	<p>A new technique, based on the exploitation of DPS4D ionosondes, is implemented to directly identify TID in real-time. For the real-time detection and evaluation of TIDs remote-sensing data from synchronized, network coordinated HF sounding between pairs of DPS4D ionosondes are exploited.</p> <p><i>(Reinisch et al., 2017; Huang et al., 2016)</i></p>
<b>HF Interferometry method</b>	<p>The method identifies coherent TID activity at different sites and sets bounds to time intervals for which such activity occurs into a given region.</p> <p><i>(Altadill et al., 2017)</i></p>
<b>TID activity monitoring using GNSS data</b>	<p>TEC observations used for the analysis are calculated utilizing L1 and L2 Global Positioning Systems (GPS) frequency measurements (i.e. 1575.42 and 1227.60 MHz, respectively) in an algorithm developed at Boston College.</p>

## TechTIDE project network (including possible extension)



### 1D Altitude profile of TID

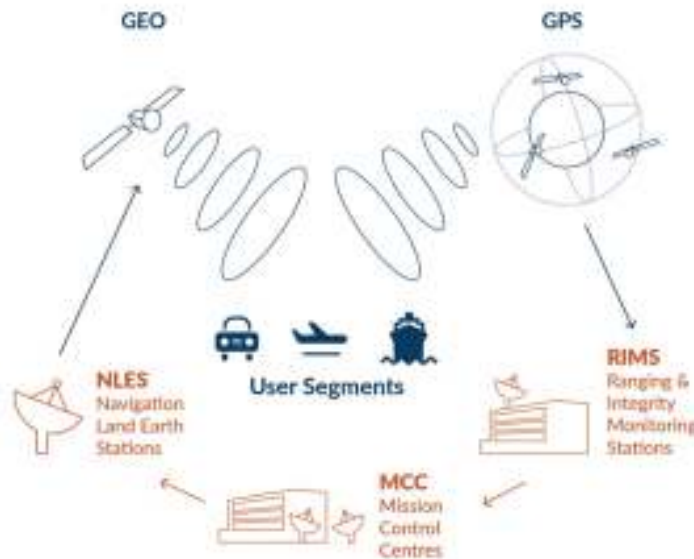
- Detailed view of propagation along z-axis
- Pin-point to particular altitude region

### Sensitivity (amplitude)

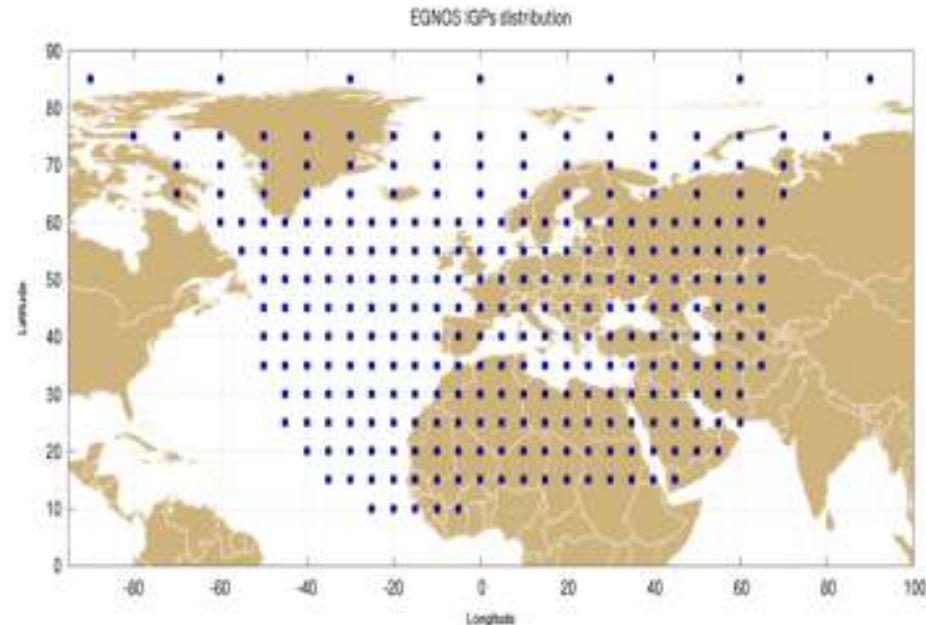
- Detection of a 5% TID vs underlying density
- “TID are always present” < 2%

### Direction, Velocity, Wavelength

- Direct measurement
- Static platform
- No geometric transformation needed
- 24/7 operations with automatic intelligent system analysis



Scheme of EGNOS infrastructure



The map of IGPs where EGNOS computes the ionospheric corrections

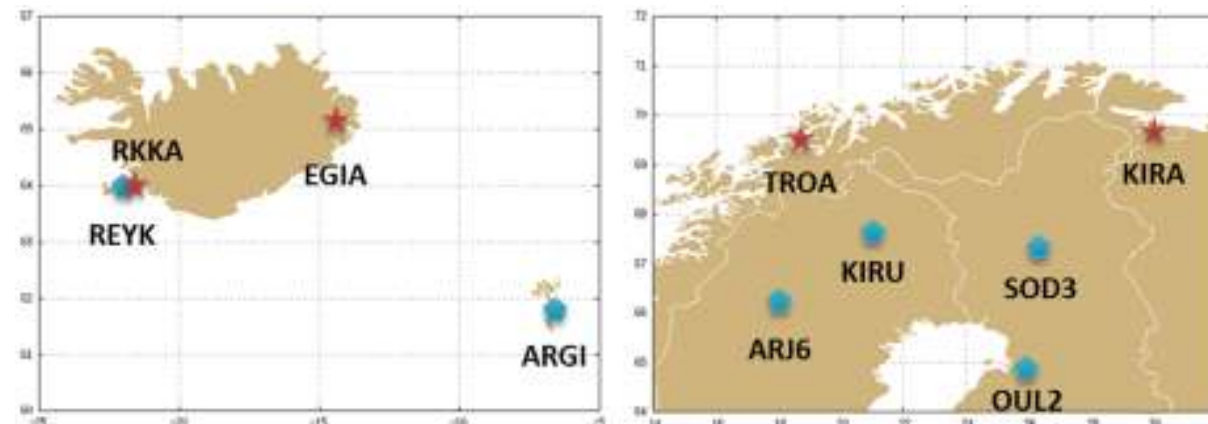
The **European Geostationary Navigation Overlay Service (EGNOS)** is Europe's regional satellite-based augmentation system (SBAS). EGNOS computes the ionospheric information distributed in a grid of pierce points, called **Ionospheric Grid Points (IGP)**, located at an altitude of 350 km over the WGS 84 ellipsoid.

The ionospheric information provided by EGNOS is:

- **Grid Ionospheric Vertical Delay (GIVD)**: Ionospheric vertical delay at the IGP for L1 frequency;
- **Grid Ionospheric Vertical Error (GIVE)**: Ionospheric Vertical Error at the IGP.

The GIVD is related with the TEC value. This parameter indicates the delay of the signal (in meters) due to the transition through ionosphere. On the other hand, the GIVE is the bounding of the GIVD estimation, that is, is the sigma (at 99.99999%) of the ionospheric delay. Any disturbance in the ionosphere would increase the width of the distribution error around the IGP and, therefore, would lead to an increase of this value.

The **Along Arc TEC Rate (AATR) index** is computed from dual-frequency GNSS measurements and serves as an ionospheric activity indicator. The higher AATR value means the larger ionospheric perturbation is in the area.



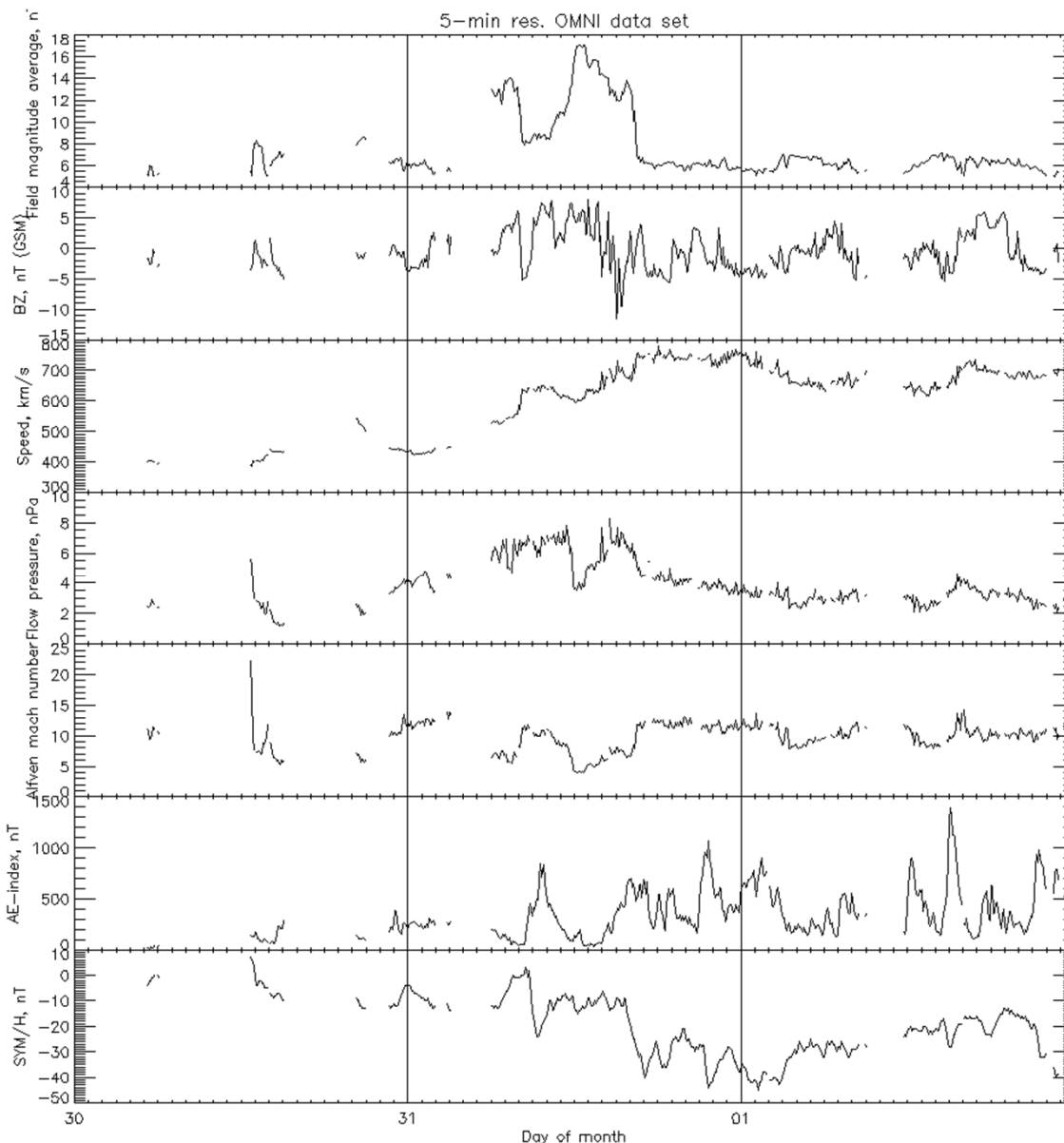
Locations of EGNOS RIMS and IGS stations

- Performance at EGNOS **Ranging Integrity Monitoring Stations (RIMS)** is computed as representative of user performance. The data used from the RIMS are:
  - EGNOS APV-I availability at RIMS;
  - Horizontal and Vertical Protection Levels (HPL and VPL, respectively).
- **IGS stations:** dual-frequency multi-constellation receivers used for the computation of the AATR values.

RIMS station	IGS station
<b>EGIA (65.1°N, 14.4°W)</b>	ARG1 (61.8°N, 6.8°W)
<b>RKKA (64.0°N, 22.0°W)</b>	REYK (64.0°N, 22.0°W)
<b>KIRA (69.6°N, 29.9°E)</b>	KIRU (67.7°N, 21.0°E)
<b>TROA (69.0°N, 18.9°E)</b>	ARJ6 (66.2°N, 18.1°E)
	OUL2 (64.9°N, 25.9°E)
	SOD3 (67.3°N, 26.4°E)

**EGNOS APV-I Availability is defined as the percentage of epochs in which the Protection Level are below Alert Limits for this APV-I service (HPL<40m and VPL<50m) over the total period.**

## 31 January -1 February 2017 event

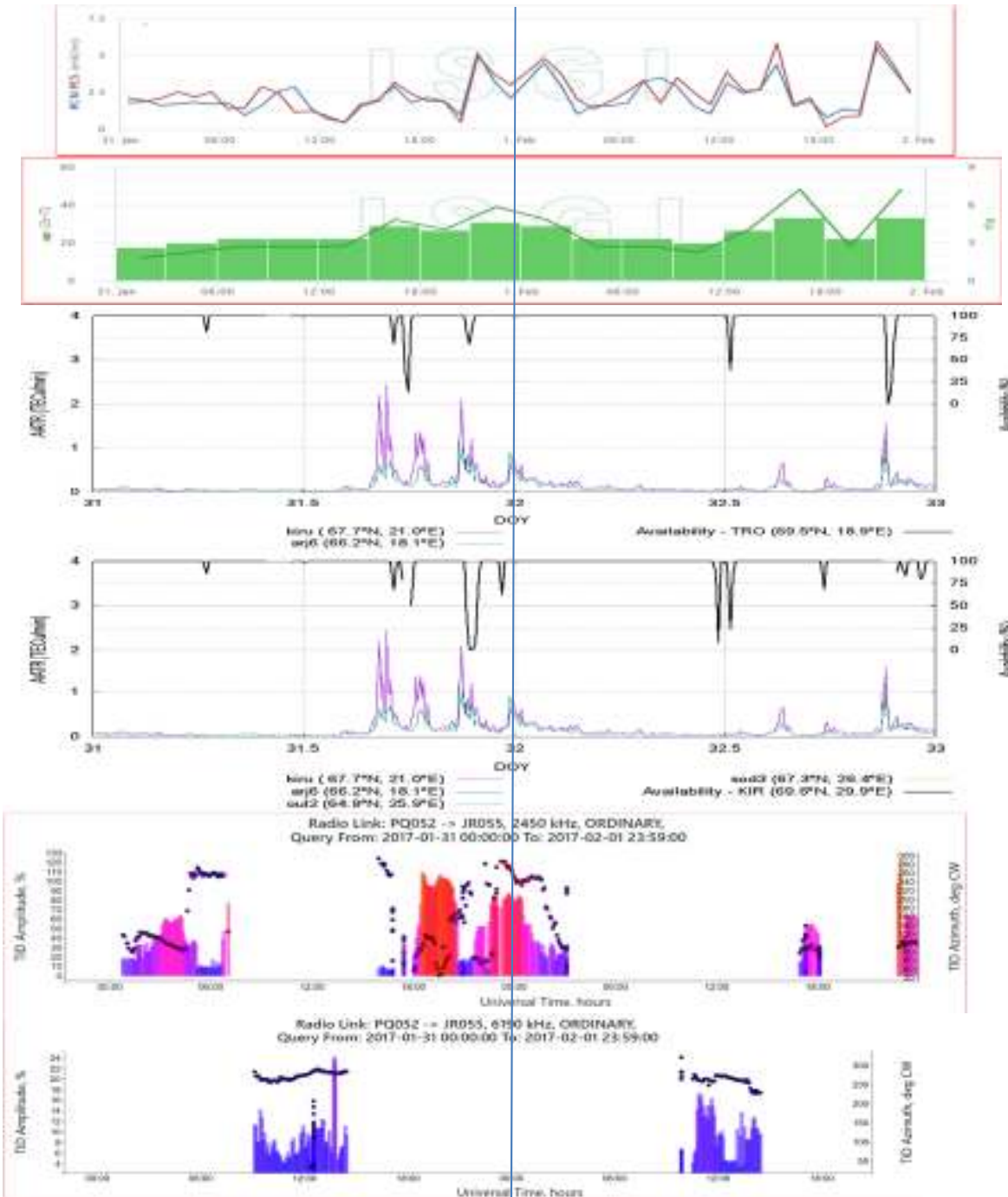


Geomagnetic field activity ranged from quiet to G1 (minor) geomagnetic storm conditions. The period began with solar wind speeds near 400 km/s. By 30/11:38 UTC, total field and solar wind speed began to increase indicating the arrival of a **CIR** followed by a negative polarity **CH HSS**. By 31/11:53, total field reached a maximum of 17.2 nT while the solar wind speed reached a peak of 796 km/s at 31/20:41 UTC. By 31/16:00 UTC, total field had decreased to 5-6 nT. The solar wind speed began to decline early on 2 February.

No Earth-directed coronal mass ejections were observed.

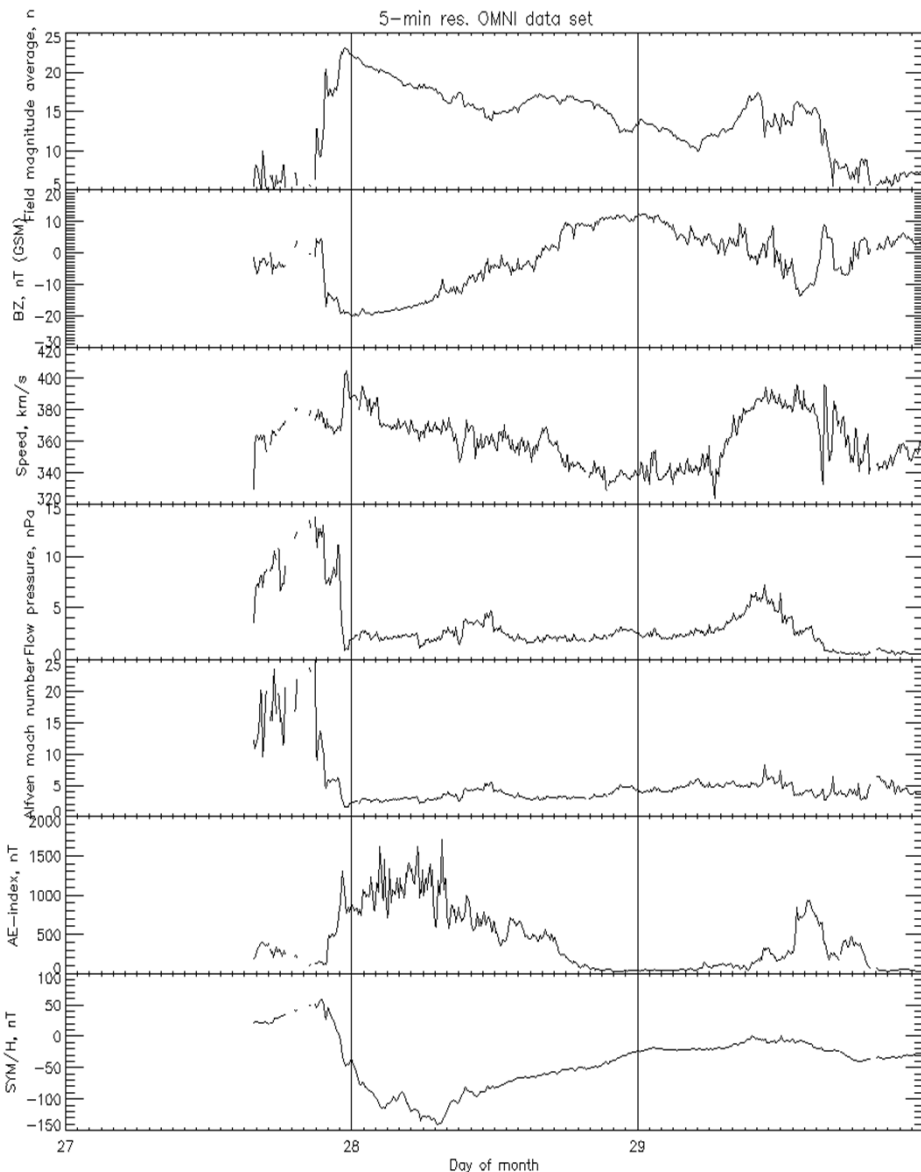
No proton events were observed at geosynchronous orbit.

## 31 January - 1 February 2017

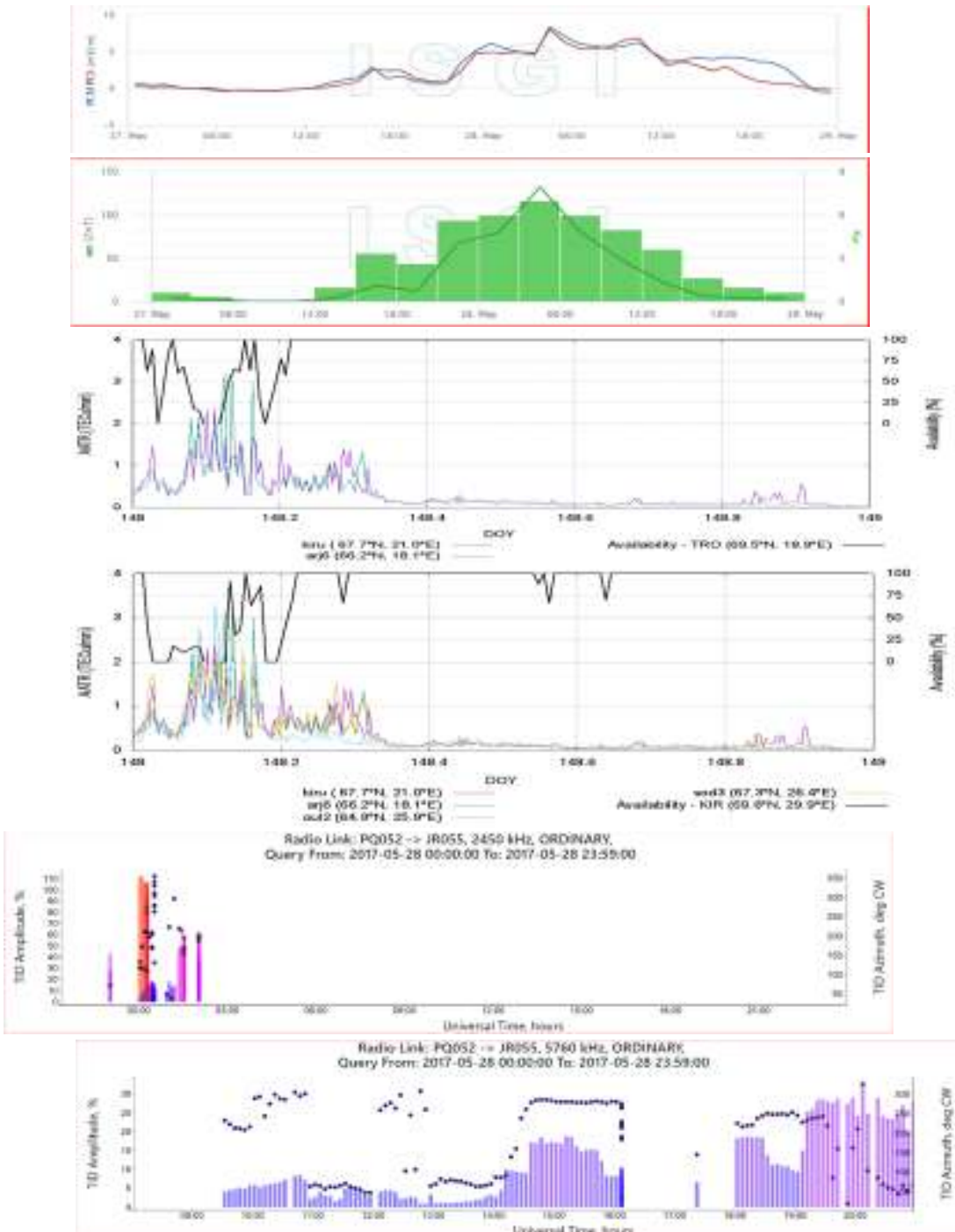


Time (UT)	WA, %	WAz, deg	WL, km	WP, min
<b>PQ-JR path (2450 kHz)</b>				
31/01/01:30-05:00	64	88	1110	155
31/01/05:00-08:00	78	126	1188	150
31/01/18:00-20:00	77	149	4270	160
31/01/20:00-24:00	83	265	2484	105
31/01-01/02/23:00-03:00	39	251	913	65
01/02/20:00-23:00	60	98	1204	115

## 28 May 2017 event



Solar wind speed was steady between 350 km/s and 380 km/s when increase in total field was observed with the transition into the magnetic cloud at 27/20:00 UTC. Total field reached a maximum of 23 nT at 27/22:30. The Bz component deflected southward to -20 nT beginning at 27/20:36 UTC and remained negative until 28/14:42 UTC. A geomagnetic sudden impulse was observed at 27/15:36 UTC (19 nT at the Boulder magnetometer) indicating the arrival of the **partial-halo CME of 23 May**. The geomagnetic field responded with a period of G2 (Moderate) storm levels late on 27 May followed by G1-G3 (Minor-Strong) storm levels through midday on 28 May. A decrease to quiet to active levels was observed during the second half of 28 May.

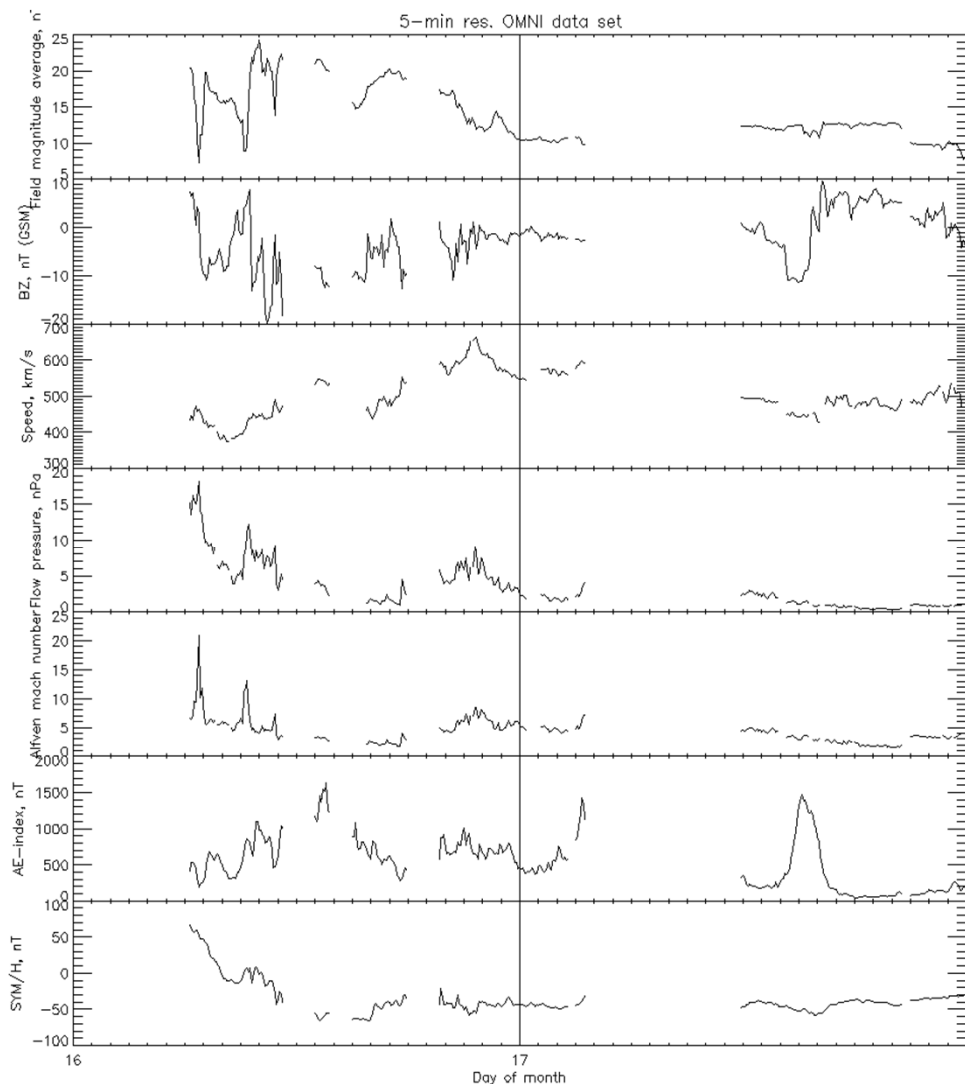


## 28 May 2017 event

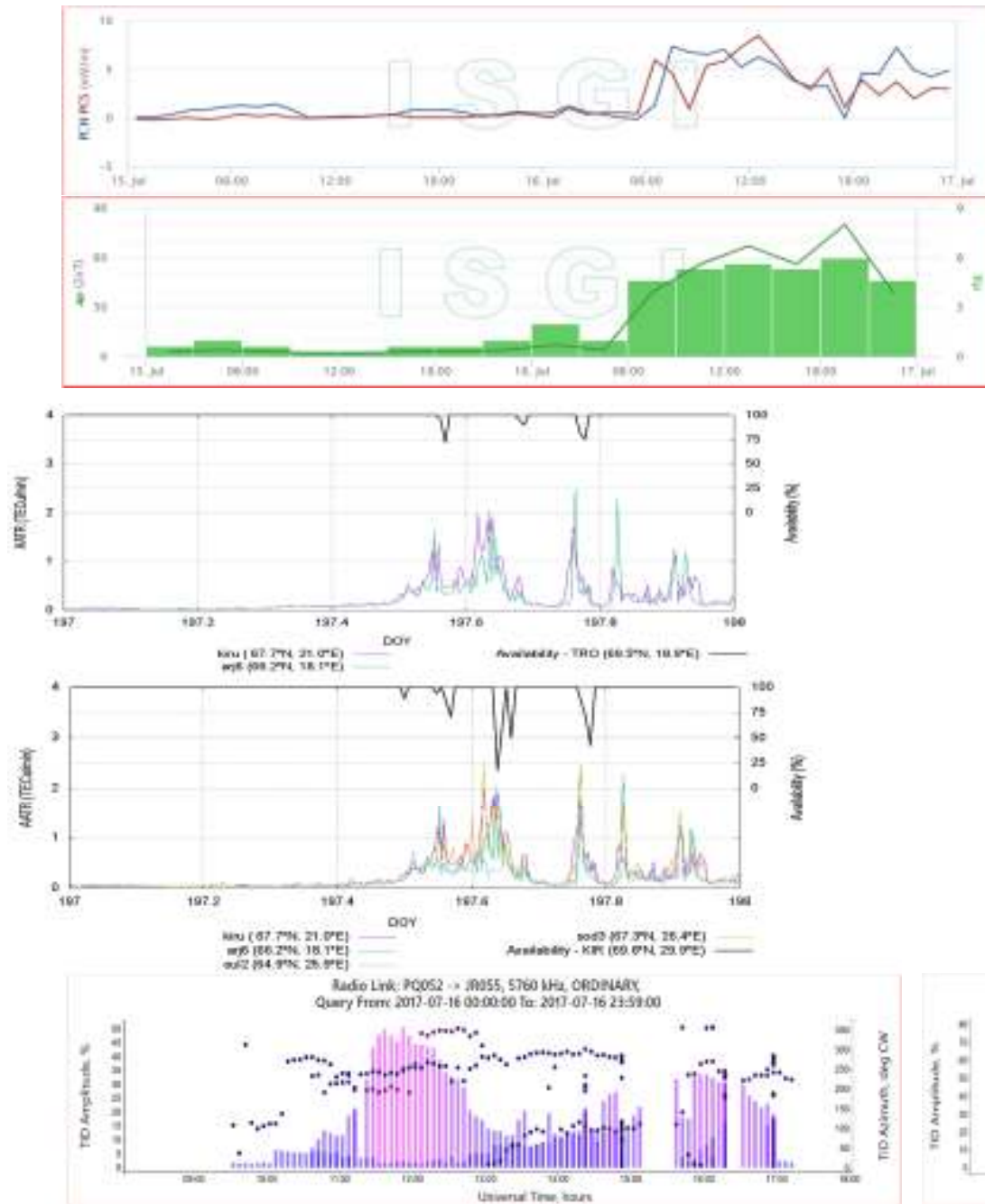
Parameters of LSTIDs observed on the PQ-JR sounding paths of 2450 KHz and 5760 KHz

Time (UT)	WA, %	WAz, deg	WL, km	WP, min
<b>PQ-JR path (2450 kHz)</b>				
27.05- 28.05/ 22:00- 00:30	84	261	3774	130
27.05- 28.05/ 23:30- 02:00	59	172	2076	120
<b>PQ-JR path (5760 kHz)</b>				
28/05/ 18:30- 22:30	28	66	330	120

## 16 July 2017 event



At 16/05:15 UTC, an interplanetary shock associated with the arrival of the **14 July CME**, was observed in DSCOVR solar wind data. Solar wind speeds sharply increased from around 320 km/s to 502 km/s and later continued slowly increasing to a peak value of 643 km/s observed at 16/20:37 UTC. Total field strength values reached 28 nT at 16/08:36 UTC while the  $B_z$  component was sustained at around -23 nT for a prolonged period following the shock arrival. The geomagnetic field was quiet until 16/06:01 UTC when a geomagnetic sudden impulse was observed (40 nT at Hartland magnetometer) indicating the arrival of the CME. The geomagnetic field responded with active to G1 and G2 (minor to moderate) geomagnetic storm levels through the remainder of 16 Jul.

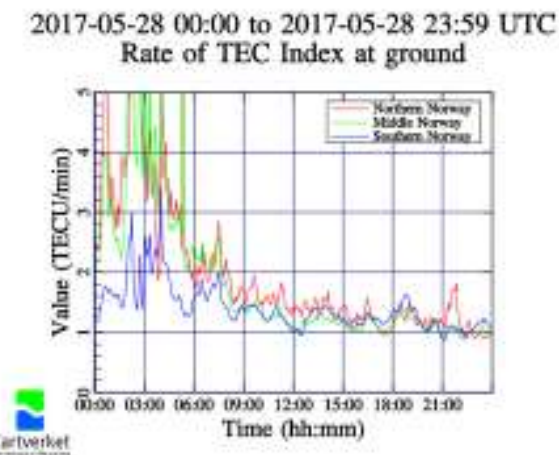
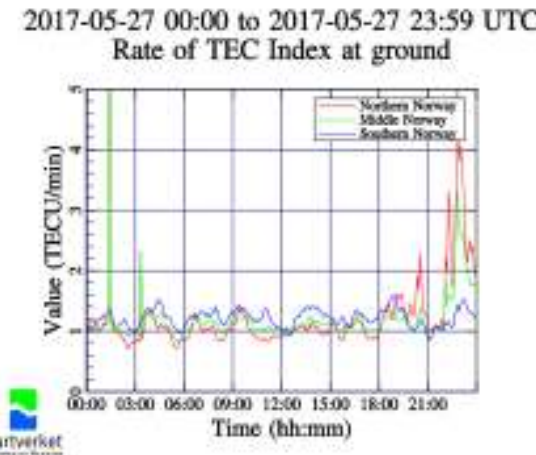
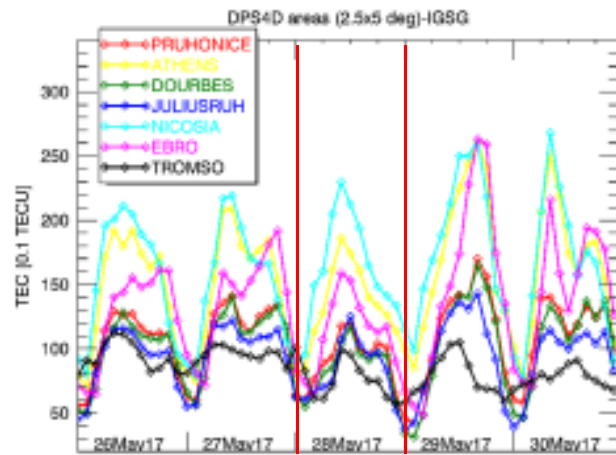


## 16 July 2017 event

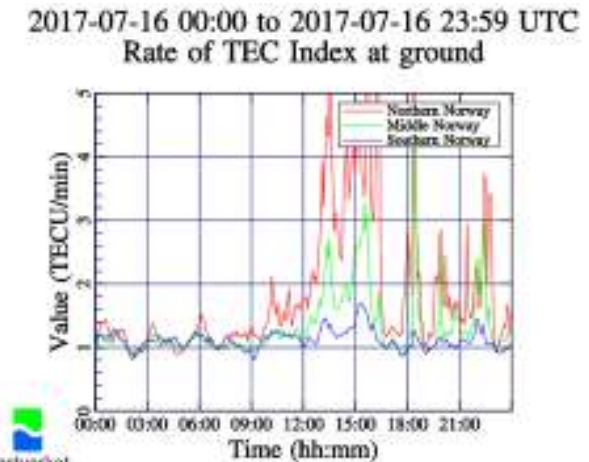
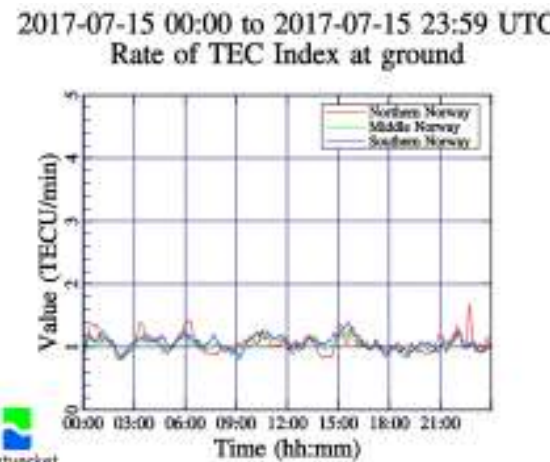
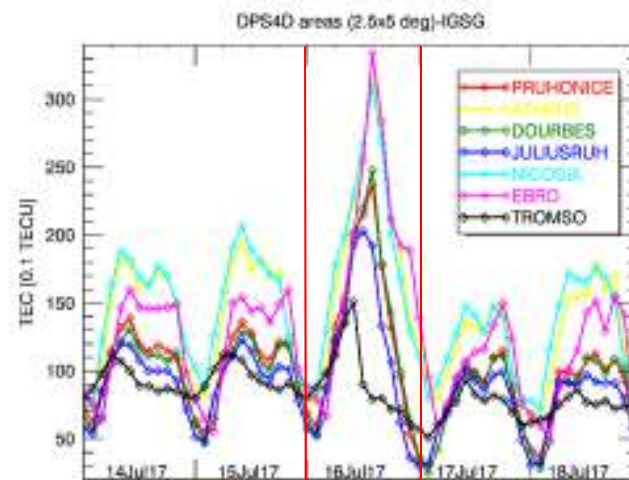
Time (UT)	WA, %	WAz, deg	WL, km	WP, min
<b>PQ-JR path (5760 kHz)</b>				
10:00-12:50	21	335	2113	78
12:30-15:10	22	111	1392	60
14:20-16:50	23	235	1148	105
<b>EB-DB path (4725 kHz)</b>				
22:40-23:55	80	117	1705	135
<b>EB-AT path (4725 kHz)</b>				
21:30-23:50	51	111	2021	56



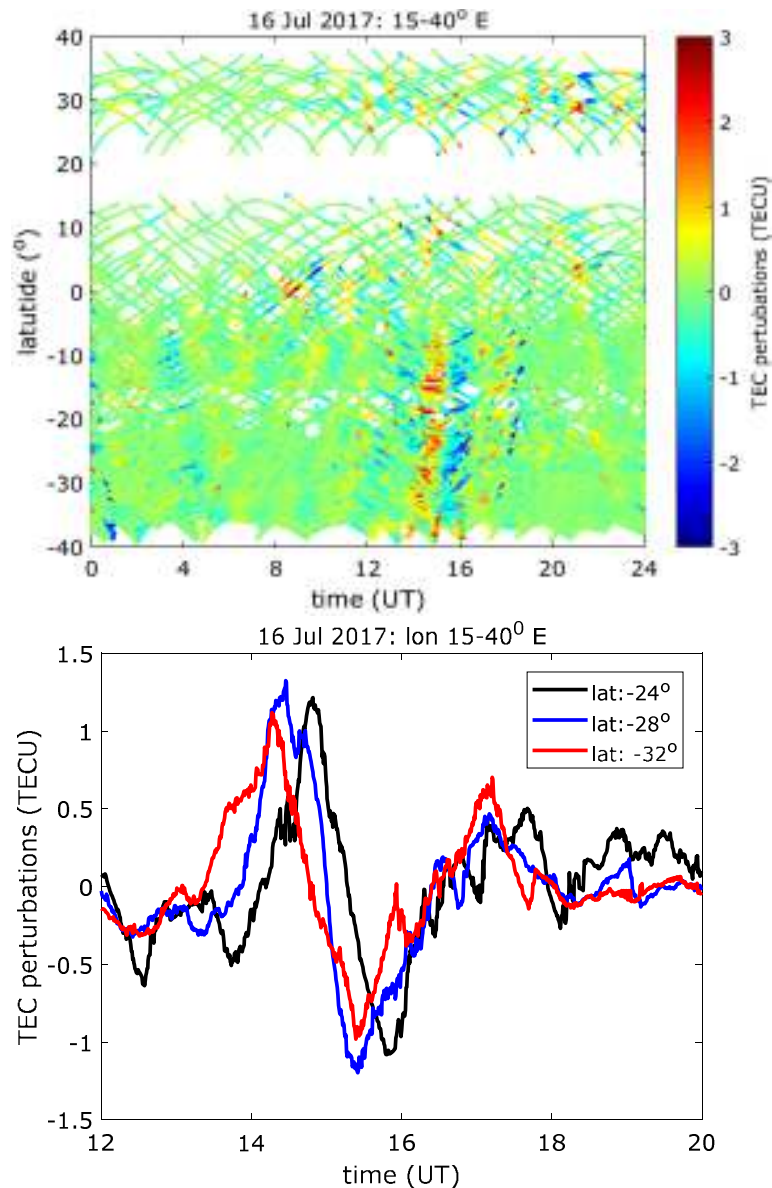
## 28 May 2017 event



## 16 July 2017 event



## LSTIDs observed over both hemispheres based on GNSS data for 16 July 2017



Map of TEC perturbations over South Africa show TID observed between 14:00 and 18:00 UT during the storm's main phase.

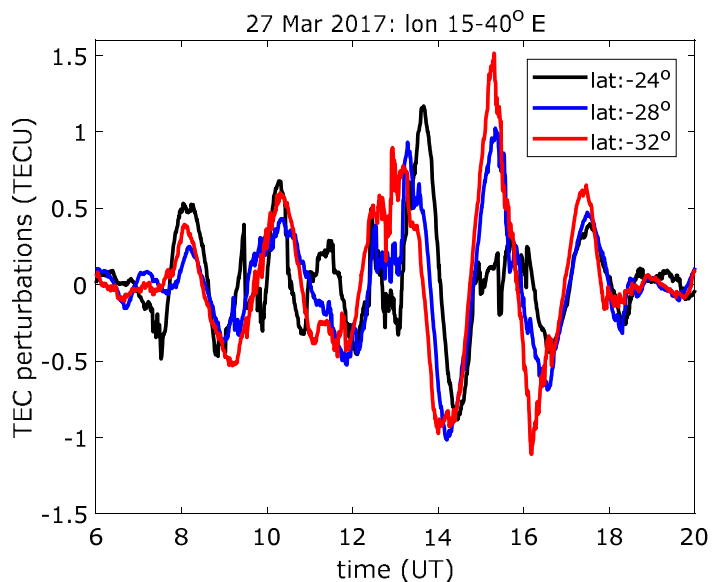
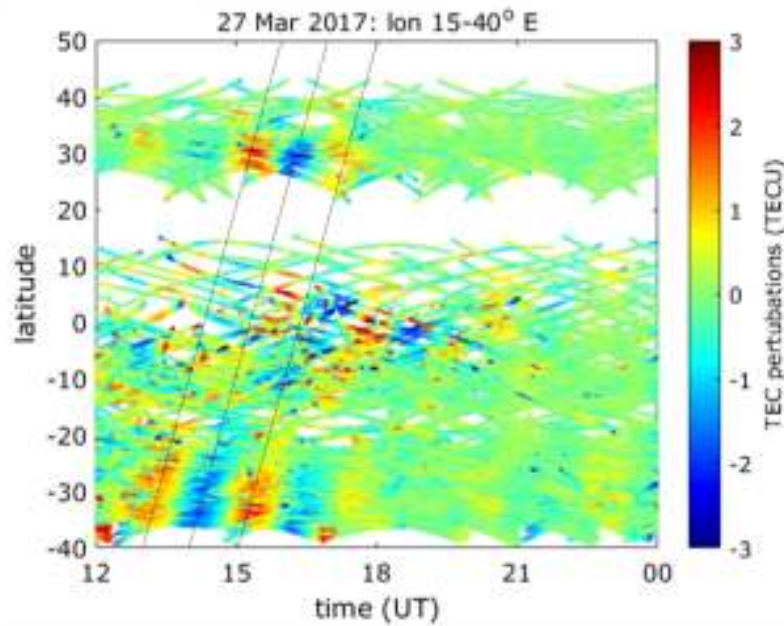
Observed TID propagating equatorward over the southern middle latitudes and dissipate in the equatorial region.

Sampled TEC perturbations at three different latitudes in order to estimate horizontal propagation speed:

- Succession of peak appearance with latitude around 14 UT confirms equatorward propagation;
- Mean speed = 418.7 m/s.

Period of the LSTID is roughly 3 hours.

## LSTIDs observed over both hemispheres based on GNSS data for 27 March 2017



The slant TEC is mapped to vertical TEC by using a thin shell model at ionospheric altitude of 350 km. In order to reduce the impact of multi-path, only data from satellites with elevation angle 30° are used.

Map of TEC perturbations over African southern middle latitudes shows TID activity between 8:00 and 20:00 UT that is intensified between 12:00 and 16:00 UT.  
TID propagating equatorward.

LSTID amplifies during course of main phase of the storm:

Mean velocity = 772 m/s  
Period of wave roughly 2 hours

APV-I 99% Availability Degraded Area  
**10.5% -moderate degradation**

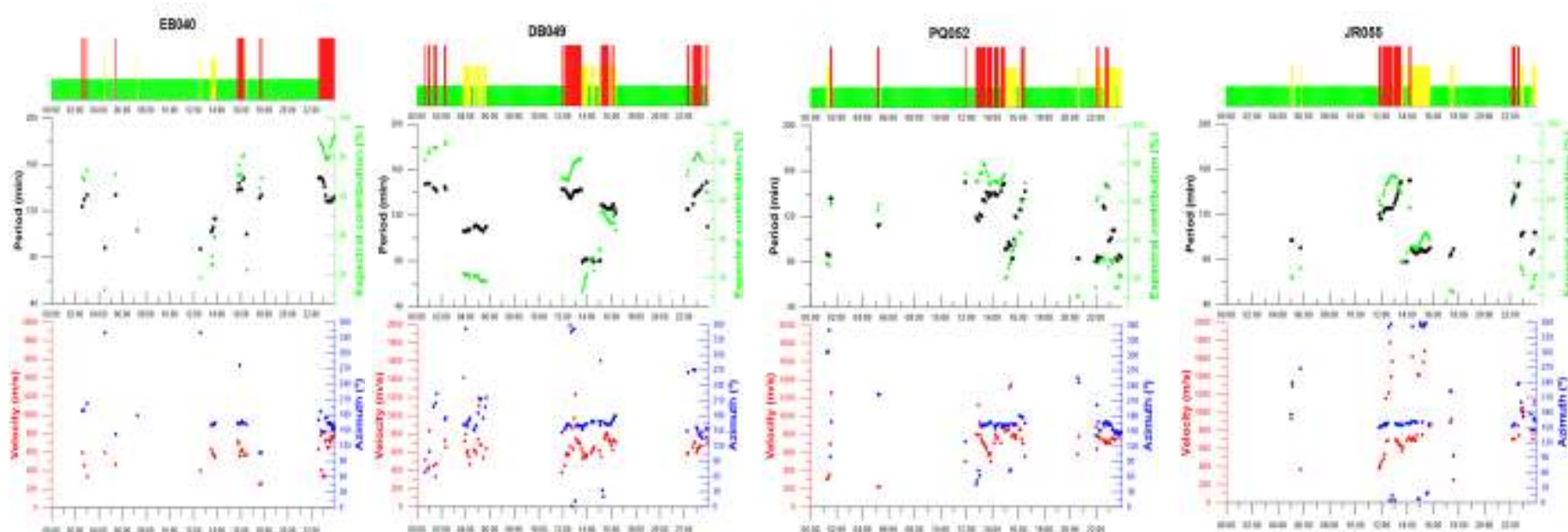
# Comparison of the results of the HF Interferometry and HF-TID techniques

## 16 July 2017

### HF-TID

Path	Time, UT	Frequency, kHz	WA, %	WAz, deg	WL, km	WP, min
EB-DB	22:40-23:55	4725	80	117	1705	135
JR-PQ	13:30-03:00	5760	33,5	264	1877	145

### HF Interferometry



## Investigation of interhemispheric circulation of LSTIDs: instruments, data and approached used

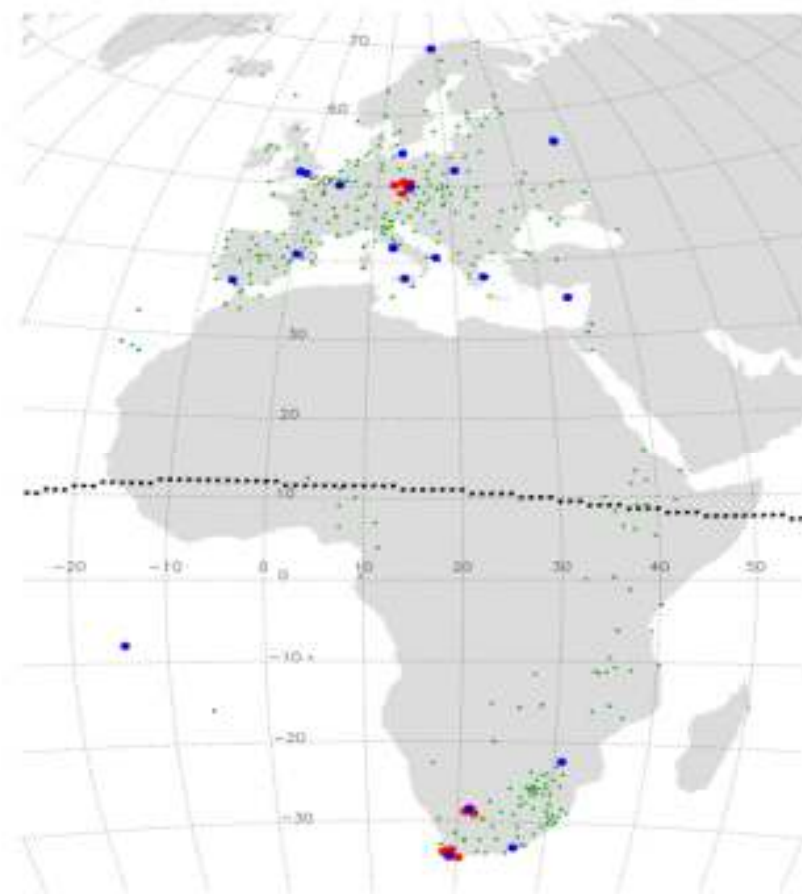
We consider LSTID with magnetospheric-ionospheric excitation mechanism, for events taken from the Project catalogue. We analyzed 38 events in total.

Neither did we consider the detailed nature of the physical processes which led to the TID nor did we distinguish TID according to the intensity, we rather employed a binary (yes/no) assessment of occurrence.

For detection and characterization we relied entirely on GPS products from ground based receivers in Europe and South Africa.

We further considered the global geomagnetic storm indices  $Dst$  and  $SYM-H$ , the local Scandinavian auroral electrojet indices  $IL$  and  $IU$ , and the northern and southern Polar Cap indices  $PCN$  and  $PCS$ .

## Instruments, data approached used to investigate interhemispheric circulation of LSTIDs



We employed exclusively **TEC data products** (TEC, dTEC, and ROT) for LSTID observations.

**TEC** was derived using the IGS, UNAVCO, and TrigNet networks of ground-based GNSS receivers in Europe and Africa and is given in TECU (1 ECU=10<sup>16</sup>e<sup>-1</sup>/m<sup>2</sup>).

**dTEC** is the difference between unsmoothed TEC observations and a TEC reference level specified as a 1-hour running mean of the unsmoothed data (DLR) or polynomial smoothing (SANSA).

**Blue dots:** Digisondes (not all were fully operational at the time of writing this report).

**Red dot groups:** HF Doppler sounder systems.

**Green dots:** GPS receiveres of the IGS, UNAVCO and TrigNet GNSS networks. Note that stations are sparse in the Sahara zone and practically absent in the sub-Sahara zone.

Dotted line across Africa means the geomagnetic equator.

We address two principal questions, namely:

- (i) what is the likeliness that LSTID occur simultaneously in both hemispheres (**hemispheric conjugacy**),
- (ii) what is the likeliness that LSTID launched in one hemisphere propagate across the equator into the other hemisphere (**interhemispheric circulation**).

## Appearance of LSTIDs in both hemispheres and interhemispheric circulation

**38** TID events from the TechTIDE project event catalogue were analysed

**26** events indicated LSTID occurrence

The 26 events in detail (each of the three groups below sums up to 26)



**16** events: LSTID in both hemispheres, no interhemispheric propagation

**4** events: interhemispheric propagation of LSTID

**6** events: LSTID occurrence in one hemisphere (insufficient data coverage of the other hemisphere)

NOTE: no case of LSTID observed in one hemisphere and definitely excluded in the other one

**14** events: LSTID originating at high latitudes and propagating equatorward

**3** events: LSTID originating near the geomagnetic equator and propagating poleward

**9** events: LSTID origination at high latitudes and near the geomagnetic equator

**13** events: LSTID during stronger storms ( $SYM-H$  exceeding -90 nT) during or immediately after the main phase

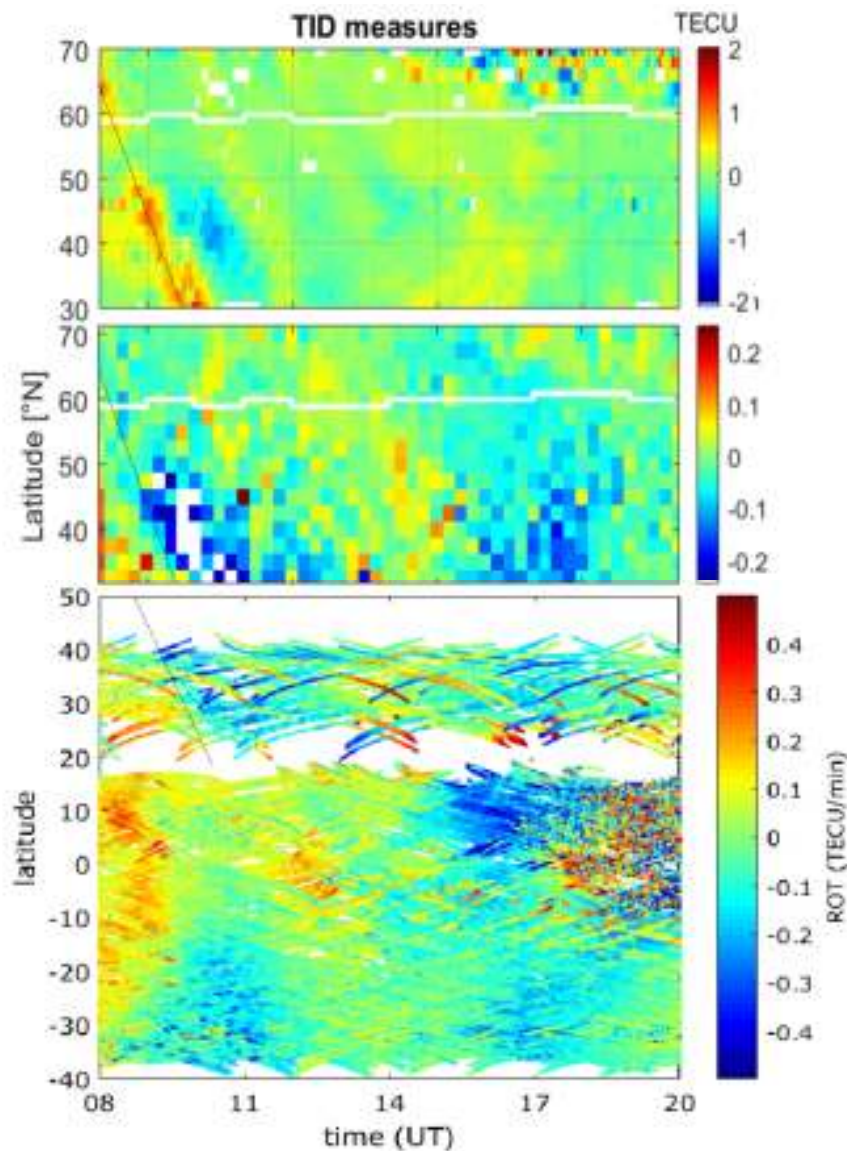
**8** events: LSTID during weak storms ( $SYM-H$  not exceeding -90 nT)

**5** events: LSTID during absence of storm conditions or late in the recovery phase of a storm

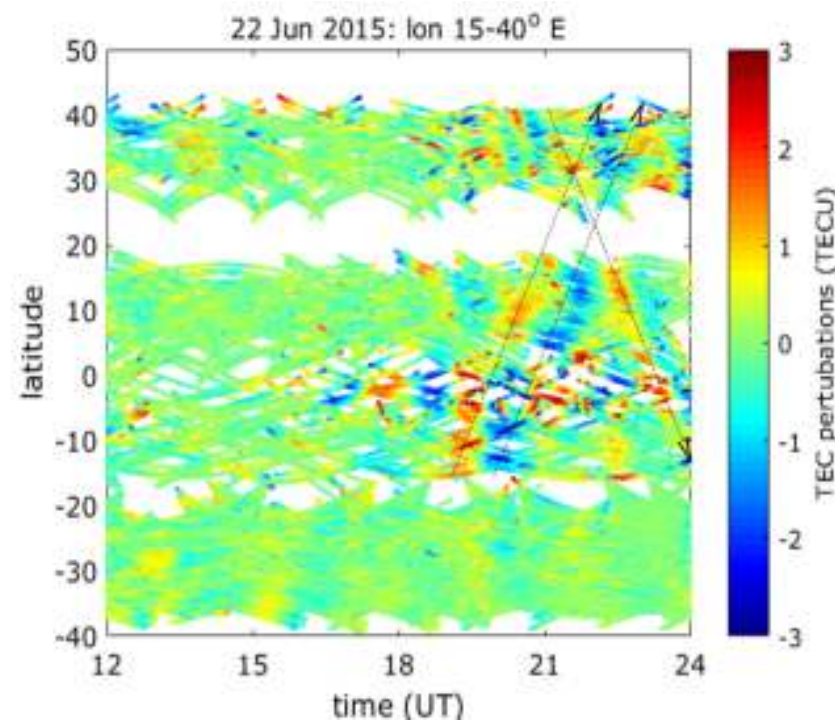
The remaining **12** events

**4** events: no LSTID during weak storm periods ( $SYM-H$  not exceeding -90 nT)

**8** events: no LSTID during storm periods or later in the storm recovery phase



TEC (top panel) and ROT (middle and bottom panels) on **2 October 2013** over the European-African longitude sector. The interval starts 1.5 hours after the end of the main phase of a moderate geomagnetic storm ( $\text{SYM-H} \approx -90 \text{ nT}$ ).



Three equatorward propagating LSTID on **22 June 2015** entering at about 13 hours after the end of the main phase of a severe geomagnetic storm ( $\text{SYM-H} \approx -200 \text{ nT}$ ) the opposite hemisphere without any particular sign of interference when the recovery phase was well underway.  
 Latitude is geographic. The geomagnetic equator is located at about  $10^\circ$  north of the geographic equator.

## Summary of what we observed:

TID driver	Number of analysed events	Magnitude of EGNOS availability degradation	Range of EGNOS availability degradation
CME	5	<b>2 - high degradation</b> <b>2 – moderate degradation</b> <b>1 – low degradation</b>	<b>22.7% - 33.9%</b> <b>8.7% - 12.0%</b> <b>1.8%</b>
CIR/CH HSS	25	<b>23 – moderate degradation</b> <b>2 – low degradation</b>	<b>5.4% - 15.7%</b> <b>4.1% - 4.3%</b>
SSBS	1	moderate degradation	6.8%

- Both CME- and CIR/HSSS-related events are significant sources of the LSTIDs.
- The CIR/HSSS-related LSTID activity has longer duration.

# ACKNOWLEDGEMENTS

---

This work has been partly developed by the TechTIDE project, funded by the European Union



Contract N° 776011

Program COMPET-5  
Space Weather

Horizon 2020 Research  
and Innovation



The logo features a stylized yellow and blue swoosh above the text "TechTIDE". Below it, the full name of the project is written: "Warning and Mitigation Technologies for Travelling Ionospheric Disturbances Effects". To the left of the text, there is contact information: "Contact: [www.tech-tide.eu](http://www.tech-tide.eu), [techtide.project@gmail.com](mailto:techtide.project@gmail.com), [@tech\\_TIDE". Further down, it says "Funded by:" followed by the "HORizon 2020" logo and "COMPET – Space Weather 2017".](https://twitter.com/tech_TIDE)

## CONSORTIUM

	National Observatory of Athens (NOA)
	Deutsches Zentrum für Luft- und Raumfahrt (DLR)
	Ustav Fyziky Atmosféry AV CR (IAP)
	Institut Royal Meteorologique de Belgique (RMI)
	Observatorio del Ebro Fundacion (OE)
	Borealis Global Designs Ltd. (BGD)
	Leibniz Institute of Atmospheric Physics, Rostock University (L-IAP)
	Universitat Politècnica de Catalunya (UPC)
	European Satellite Services Provider (ESSP)
	South Africa National Space Agency (SANSA)
	Watermann Juergen Friedrich Wilhelm (JFWCONSULT)
	Frederick University (FU), Cyprus
	German Federal Police (GFP)